PERGAMON

International Journal of HEAT and MASS TRANSFER

International Journal of Heat and Mass Transfer 42 (1999) 739–751

The effects of inlet turbulence on the development of fluid flow and heat transfer in a helically coiled pipe

C. X. Lin, M. A. Ebadian*

Florida International University, Hemispheric Center for Environmental Technology, Miami, FL 33199, U.S.A.

Received 8 April 1997; in final form 4 June 1998

Abstract

In this paper, the effects of inlet turbulence level on the development of three-dimensional turbulent flow and heat transfer in the entrance region of a helically coiled pipe are investigated by means of a fully elliptic numerical study. The k–ε standard two-equation turbulence model is used to simulate turbulent flow and heat transfer, which are assumed to develop from the inlet to the outlet simultaneously. Constant wall temperature and uniform inlet conditions are applied. The governing equations are solved by a Control-Volume Finite Element Method with an unstructured nonuniform grid system. Numerical results presented in this paper cover a Reynolds number range of 10^4–10^5, a Prandtl number range of 0.02–100, and an inlet turbulence intensity range of 2–40%. The development of the main velocity field, the secondary velocity field, the temperature field, bulk turbulent kinetic energy, the average friction factor, and average Nusselt numbers are discussed. It is found that bulk turbulent kinetic energy far from the entrance is not affected by the inlet turbulence level. Significant effects of the inlet turbulence level on the development of the friction factor and Nusselt number occur within a short axial distance from the entrance only. © 1998 Elsevier Science Ltd. All rights reserved.

Nomenclature

a radius of the helical pipe [m]
A area [m^2]
A_T Van Driest constant
C_p specific heat under constant pressure [J kg^{-1} K^{-1}]
$C_{\varepsilon 1}$, $C_{\varepsilon 2}$, C_μ turbulence model constants
d_h hydraulic diameter of the helical pipe [m]
E empirical constant in logarithmic velocity profile
f_m circumferential average friction factor on one cross section

$$\left(=\frac{1}{2\pi}\int_0^{2\pi} f_\theta \,\mathrm{d}\theta\right)$$

f_θ local friction factor on the circumference of a pipe $[=\tau_w/(0.5\rho u_0^2)]$
I turbulence intensity $(=u'/u\times 100\%)$
k turbulent kinetic energy [m^2 s^{-2}]
k_b nondimensional bulk turbulent kinetic energy on one cross section

$$\left(=\frac{1}{u_0^2\bar{u}_s A}\int_0^A u_s k \,\mathrm{d}A\right)$$

L characteristic turbulence length scale [m]
n coordinate direction perpendicular to a surface
Nu_m circumferential average Nusselt number on a cross section

$$\left(=\frac{1}{2\pi}\int_0^{2\pi} Nu_\theta \,\mathrm{d}\theta\right)$$

Nu_θ local Nusselt number on the circumference of a pipe $(=(q_w d_h/\Gamma_l)/(T_w-T_b))$
p pressure [N m^{-2}]
Pr molecular Prandtl number
Pr_w turbulent wall Prandtl number
q_w local heat flux [W m^{-2}]
r radial coordinate [m]
R_c radius of the coil [m]
Re Reynolds number $(=\rho u_0 d_h/\mu)$
s axial coordinate [m]
T temperature [K]
T_b fluid bulk temperature on one cross section

* Corresponding author

0017–9310/98 $19.00 © 1998 Elsevier Science Ltd. All rights reserved
PII: S0017–9310(98)00193–8

$\left(=\dfrac{1}{\bar{u}_s A}\int_0^A u_s T\,\mathrm{d}A\right)$ [K]

u velocity component in the flow direction [m s^{-1}]
u' root-mean-square turbulent velocity fluctuation [m s^{-1}]
u_0 inlet velocity [m s^{-1}]
u_i velocity component in the i-direction ($i = 1, 2, 3$) [m s^{-1}]
u^* friction velocity ($=\sqrt{\tau_w/\rho}$) [m s^{-1}]
U_s nondimensional axial velocity ($=u_s/u_0$)
x_i Cartesian coordinate in the i-direction ($i = 1, 2, 3$) [m].

Greek symbols
α angle [°]
Γ thermal conductivity [W/(m·K)]
Γ_{eff} effective thermal conductivity [W/(m·K)]
δ_{ij} Dirac delta function
ε dissipation rate of turbulent kinetic energy [m^2 s^{-3}]
φ axial angle [°]
κ Von Karman constant
μ viscosity [kg m^{-1} s^{-1}]
Θ nondimensional temperature ($=(T-T_w)/(T_b-T_w)$)
ρ density of the fluid [kg m^{-3}]
σ_T turbulent Prandtl number in energy equation
σ_k diffusion Prandtl number for k
σ_ε diffusion Prandtl number for ε
τ_w wall shear stress [N m^{-2}].

Superscripts
$-$ average
$'$ fluctuation
$+$ standard wall coordinates.

Subscripts
0 inlet conditions
b bulk quantity
i, j, k general spatial indices
l laminar or molecular quantity
r, θ, s radial, azimuthal, and axial directions, respectively
t turbulent quantity
w wall condition.

1. Introduction

Turbulent fluid flow and heat transfer in a helically coiled pipe of constant circular cross section are of interest in fundamental studies and of importance in many engineering applications, such as compact heat exchangers, evaporators, condensors, chemical reactors, storage tanks and piping systems. Most of the previous studies on this topic have been carried out within the regime of fully developed turbulent flow or heat transfer by means of experimental methods. Experimental studies after 1980 include those by Kalb and Seader [1]; Mikaila and Poskas [2]; Belenkiy et al. [3]; Webster and Humphrey [4]; Das [5]; and Rao [6,7]. Few studies have been conducted using numerical methods due to the geometrical and mathematical difficulties in describing and solving the physical problem. Moreover, although the inlet boundary conditions do play an important part in developing turbulent flow and heat transfer in the entrance region of helically coiled pipe, no extensive data on the effects of inlet boundary conditions are available in the open literature, particularly regarding the effects of inlet turbulence.,

Among the numerical studies, Patankar et al. [8] applied the standard k–ε two-equation turbulence model to predict turbulent developing fluid flow in curved pipes, but only fully developed hydrodynamic results were reported for helically coiled pipes. Yang and Ebadian [9] adopted the same turbulence model to investigate fully developed turbulent heat transfer in helical pipes with substantial pitch. Both of these numerical studies used the Control-Volume Finite Difference Method developed by Patankar and Spalding [10], a method which is of first-order accuracy. These two studies also treated the flow as parabolic; the diffusion fluxes in the axial direction together with terms of small order of magnitude in governing equations were neglected. Recently, Lin and Ebadian [11,12] performed fully elliptic computations of developing turbulent flow and heat transfer in helical pipes by means of a Control-Volume Finite Element Method, which is of second-order accuracy. The development of turbulent flow and heat transfer in helical pipes with finite pitch were addressed in their investigations.

It is well known that the standard k–ε two-equation turbulence model is based on an isotropic eddy-viscosity concept. Robustness, economy, and reasonable accuracy for a wide range of turbulent flows have explained its popularity in engineering applications. Although concerns may arise when flows with streamline curvature and secondary velocity are considered, the reported good agreement [8,9,11,12] between numerical predictions by the standard turbulence model and available experimental results indicates that the standard turbulence model can be applied in the modeling of turbulent flows in coiled pipes within certain parameter ranges.

In this paper, the effects of inlet turbulence level on the development of turbulent flow and heat transfer in a helically coiled pipe are investigated with the standard k–ε turbulence model. To capture the physics of three-dimensional fluid flow and heat transfer in the coiled pipe, fully elliptic flow computations have been performed with a Control-Volume Finite Element Method of second-order accuracy.

2. Physical problem

The geometry and physical problem considered are shown in Fig. 1. The circular pipe studied, which has a

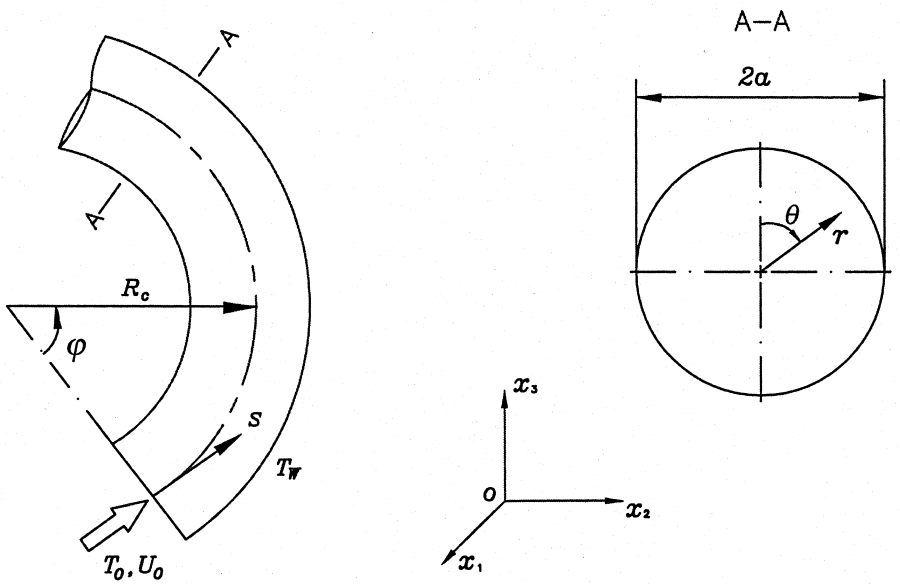

Fig. 1. Physical problem.

diameter of $2a$, is coiled at a radius of R_c. At the inlet ($\varphi = 0^\circ$), fluid with turbulence intensity I and temperature T_0 enters into the coiled pipe at a speed of u_0. The wall of the pipe is heated under temperature T_w. Turbulent flow and heat transfer develop simultaneously downstream in the coiled pipe. The k–ε turbulence model developed by Launder and Spalding [13] is used to simulate the turbulent flow. Reynolds stresses are related to the mean velocity gradients on the basis of the Boussinesq hypothesis. Turbulent heat flux in the energy equation is modeled using the gradient transport analogy. The present analysis of the physical problem does not include the buoyancy effects. The time-averaged, fully elliptic differential equations governing the steady turbulent flow in the coiled pipe can be written in tensor form as:

Mass:

$$\frac{\partial u_i}{\partial x_i} = 0 \tag{1}$$

Momentum:

$$\frac{\partial}{\partial x_j}\left[\mu_l+\mu_t)\left(\frac{\partial u_i}{\partial x_j}+\frac{\partial u_j}{\partial x_i}-\delta_{ij}\frac{2}{3}\frac{\partial u_k}{\partial x_k}\right)-\rho u_j u_i-\delta_{ij}p\right] = 0 \tag{2}$$

Energy:

$$\frac{\partial}{\partial x_j}\left[\left(\Gamma_l+\frac{\mu_t C_p}{\sigma_T}\right)\frac{\partial T}{\partial x_j}-\rho u_j C_P T\right]+\mu_l\Phi_v+\rho\varepsilon = 0 \tag{3}$$

Turbulent kinetic energy:

$$\frac{\partial}{\partial x_j}\left[\left(\mu_l+\frac{\mu_t}{\sigma_k}\right)\frac{\partial k}{\partial x_j}-\rho u_j k\right]+\rho P-\rho\varepsilon = 0 \tag{4}$$

Dissipation rate of turbulent kinetic energy:

$$\frac{\partial}{\partial x_j}\left[\left(\mu_l+\frac{\mu_t}{\sigma_\varepsilon}\right]\frac{\partial\varepsilon}{\partial x_j}-\rho u_j\varepsilon\right]+C_{\varepsilon1}\frac{\rho\varepsilon P}{k}-C_{\varepsilon2}\frac{\rho\varepsilon^2}{k} = 0 \tag{5}$$

where

$$P = \frac{\mu_t}{\rho}\frac{\partial u_i}{\partial x_j}\left(\frac{\partial u_i}{\partial x_j}+\frac{\partial u_j}{\partial x_i}\right) \tag{6}$$

$$\Phi_v = \frac{\partial u_i}{\partial x_j}\left(\frac{\partial u_i}{\partial x_j}+\frac{\partial u_j}{\partial x_i}-\frac{2}{3}\frac{\partial u_k}{\partial x_k}\delta_{ij}\right) \tag{7}$$

In the above equations, the subscripts i, j, $k = 1, 2, 3$. Turbulent kinetic energy, k, and its dissipation rate, ε, are coupled to the governing equations via the relation $\mu_t = \rho C_\mu k^2/\varepsilon$. The empirical constants for the turbulence model are assigned the following values in accordance with the recommendation by Launder and Spalding [13]:

$C_\mu = 0.09$, $C_{\varepsilon1} = 1.47$, $C_{\varepsilon2} = 1.92$,
$\sigma_T = 0.7$, $\sigma_k = 1.0$, $\sigma_\varepsilon = 1.3$

To represent the results, the following nondimensional variables and parameters are defined:

$$Re = \frac{\rho u_0 d_h}{\mu}, \quad k_b = \left(\frac{1}{\bar{u}_s A}\int_0^A u_s k\,dA\right)\frac{1}{u_0^2}$$

$$U_s = \frac{u_s}{u_0}, \quad U_{2nd} = \frac{(u_r^2+u_\theta^2)^{1/2}}{u_0}$$

$$f_\theta = \frac{\tau_w}{\frac{1}{2}\rho u_0^2}, \quad f_m = \frac{1}{2\pi}\int_0^{2\pi} f_\theta\,d\theta$$

$$T_b = \frac{1}{\bar{u}_s A}\int_0^A u_s T\,dA, \quad \Theta = \frac{T-T_w}{T_b-T_w}$$

$$Nu_\theta = \frac{q_w d_h}{\Gamma_l (T_w - T_b)}, \quad Nu_m = \frac{1}{2\pi}\int_0^{2\pi} Nu_\theta \, d\theta \tag{8}$$

where U_s is nondimensional axial velocity; U_{2nd}, nondimensional secondary velocity; Θ, nondimensional temperature; k_b, nondimensional bulk turbulent kinetic energy; f_m circumferential average friction factor on one cross section; and Nu_m, circumferential average Nusselt number on one cross section.

3. Wall functions and boundary conditions

The two-layer based nonequilibrium wall function method developed by Launder and Spalding [14] is used to account for the near wall regions in the numerical computation of turbulent flow. The first near wall numerical grid point, M, is located sufficiently far from the wall for the local turbulent Reynolds number ($= \rho k^{1/2} l/\mu$, where $l = k^{3/2}/\varepsilon$) to be much greater than unity. In the region between the wall and node M, the expression for velocity is:

$$\frac{u}{u^*} = \begin{cases} y^+, & y^+ \leqslant y_v^+ \\ \dfrac{2}{\kappa}\ln(Ey^+), & y^+ > y_v^+ \end{cases}. \tag{9}$$

Here u and y denote the velocity component in the flow direction and the normal distance from the wall, respectively. The term y^+ is the dimensionless y ($y^+ = \rho u* y/\mu$); $\kappa = 0.41$; and $E = 9.793$ (for a smooth wall). The term y_v^+ represents the thickness of the viscous sublayer ($y^+ = 11.225$). Outside of the viscous sublayer, the friction velocity, defined as $\sqrt{\tau_w/\rho}$ is computed as $u* = C_\mu^{1/4} k^{1/2}$.

In the near wall cell, the value of the dissipation rate of the turbulent kinetic energy is given by:

$$\varepsilon = \frac{C_\mu^{3/4} k^{3/2}}{\kappa y}. \tag{10}$$

The turbulent kinetic energy equation is solved with zero normal derivative wall boundary conditions. The production term is computed using the velocity wall function described above to compute wall shear stress, and the dissipation at the near wall cell is obtained using an average over the cell:

$$\bar{\varepsilon} = \frac{C_\mu^{1/2} uk}{y}. \tag{11}$$

The wall heat flux is computed using $q_w = \rho C_p u* \Delta T/T^+$, where T^+ is obtained from

$$T^+ = \begin{cases} Pr\dfrac{u}{u_*}, & y^+ \leqslant y_v^+ \\ Pr_w\left(\dfrac{u}{u_*} + P_T\right), & y^+ > y_v^+ \end{cases} \tag{12}$$

$$P_T = \frac{\pi/4}{\sin(\pi/4)}\left(\frac{A_T}{\kappa}\right)^{1/2}\left(\frac{Pr}{Pr_w} - 1\right)\left(\frac{Pr_w}{Pr}\right)^{1/4} \tag{13}$$

where Pr is the molecular Prandtl number; Pr_w, the turbulent wall Prandtl number ($Pr_w = 1.2$); and A_T, the Van Driest constant ($A_T = 26$).

Among the entrance or inlet boundary conditions, only the inlet turbulence and its effects on developing flow and heat transfer in the pipe are examined in this study. Uniform profiles for all the dependent variables are used at the inlet boundary just for simplicity:

$$u_s = u_0, \quad u_r = 0, \quad u_\theta = 0, \quad T = T_0, \quad k = k_0, \quad \varepsilon = \varepsilon_0 \tag{14}$$

where u_s, u_r, and u_θ are the axial, radial, and azimuthal velocities, respectively. Turbulent kinetic energy at the inlet, k_0, and the dissipation rate of turbulent kinetic energy at the inlet, ε_0, are calculated by

$$k_0 = \frac{3}{2}(u_0 I)^2, \quad \varepsilon_0 = C_\mu^{3/4}\frac{k^{3/2}}{L}. \tag{15}$$

As the turbulent eddies cannot be larger than the pipe, the turbulence characteristic length scale, L, is set to be $0.07\,a$ in the present study. The factor of 0.07 is based on the maximum value of the mixing length in fully developed turbulent pipe flow. The turbulence intensity level, I, is defined as:

$$I = \frac{u'}{u} \times 100\%. \tag{16}$$

At the outlet, the diffusion fluxes for all variables in the exit direction are set to be zero:

$$\frac{\partial}{\partial n}(u_s, u_r, u_\theta, T, k, \varepsilon) = 0. \tag{17}$$

Nonslip and isothermal boundary conditions are imposed on the wall of the coiled pipe:

$$u_s = 0, \quad u_r = 0, \quad u_\theta = 0, \quad T = T_w. \tag{18}$$

According to Srinivasan et al. [15], Re_{crit}, the critical Reynolds number identifying a transition from laminar to turbulent flow in a curved pipe, can be estimated by

$$Re_{crit} = 2100\left[1 + 12\left(\frac{R_c}{a}\right)^{-1/2}\right] \tag{19}$$

Usually, the critical Reynolds number for a curved pipe is much higher than that for a straight pipe. In the present paper, the Reynolds numbers applied are higher than those predicted by equation (19) to ensure that the flow in the helically coiled pipe is within the turbulent regime.

4. Numerical computation

The governing equations have been solved with a Control-Volume Finite Element Method similar to that introduced by Baliga and Patankar [16]. The FLUENT/UNS

code [17] has been used as the numerical solver. As the Control-Volume Finite Element Method combines the best aspects of the Control-Volume Finite Difference Method and the Finite Element Method, it provides the mesh flexibility of the Finite Element Method without sacrificing the benefits of the Control-Volume Finite Difference Method, which are robustness and economy.

An unstructured (block-structured) nonuniform grid system is used to discretize the governing equations. Figure 2 depicts the three-dimensional grid system. Each three-dimensional hexahedral element in the grid system has 27 nodes. The distribution of the grid on the circumference of each cross section is uniform. Five blocks were applied to form the entire helically coiled pipe, with the central square block occupying 12.4% of the area on each cross section.

The convection term in the governing equations was modeled with the bounded second-order upwind scheme, and the diffusion term was computed using the multilinear interpolating polynomials $N_i(x_1, x_2, x_3)$ (also referred to as the 'shape function' in the Finite Element Method). The final discrete algebraic equation for variable ϕ at each node is a set of nominally linear equations that can be written as:

$$a_P\phi_P = \sum_{\text{nb}} a_{\text{nb}}\phi_{\text{nb}} + c_{\text{sb}} \tag{20}$$

where a_P is the center coefficient; a_{nb} is the influence coefficient for the neighbor; and c_{sb} is the contribution of the constant part of the source term S_c in $S = S_c + S_p\phi$ and of the boundary conditions. The SIMPLEC algorithm [18] is used to revolve the coupling between velocity and pressure. The algebraic equations are solved iteratively using an additive-correction multigrid method [19] with a Gauss–Seidel relaxation procedure. To accelerate convergence, the under-relaxation technique is applied to all dependent variables (the under-relaxation factor for p is 0.3; that for T is 1.0; and that for u_i, k and ε is 0.7). The numerical computation is considered to be converged when the residual summed over all the computational nodes satisfies the following criterion:

$$\frac{R^n_\phi}{R^m_{\phi,\max}} \leqslant 10^{-5} \tag{21}$$

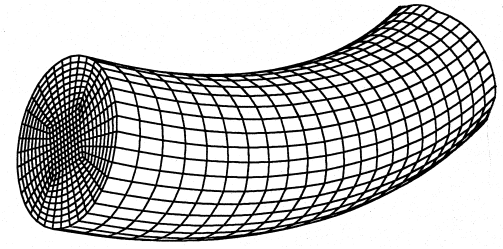

Fig. 2. Unstructured grid system for helically coiled pipe.

where R^n_ϕ is the residual at the nth iteration for variable ϕ, and $R^m_{\phi,\max}$ represents the maximum residual value after m iterations. The variable ϕ applies for u_i, T, k and ε.

In the present study, the computational domain in the axial direction extends from $\varphi = 0^\circ$ to $\varphi = 270^\circ$. The choice of this computation domain is based on the entry length data on curved pipes presented by Austin and Seader [20] to ensure that fully developed flow results can be obtained on the outlet plane. A grid independence study was carried out with grid distributions (sectional × axial) of 245×100, 320×120, 720×120, 500×120, 500×160, and 500×200. Here, the sectional number refers to the total number of elements on one cross section of the pipe. Based on the computed maximum and average values of velocity, temperature, friction factor, Nusselt number, and turbulence quantities, a grid distribution of 500×160 was found sufficient to obtain the grid-independent numerical results of turbulent flow and heat transfer. Numerical results with even finer grids are within 1% of that by the 500×160 grid. The detailed grid dependence study can be found in Lin and Ebadian [11,12].

Validation studies were also conducted for the numerical models used with the experimental data available on turbulent flow and heat transfer in coiled pipes. Numerical predictions of the velocity profiles were compared with experimental data by Mori and Nakayama [21]; numerical predictions of the friction factors were compared with experimental data by Ito [22]; and numerical predictions of Nusselt numbers were compared with experimental data by Rogers and Mayhew [23]. It has been observed that the numerical results agree fairly well with the experimental results. A detailed comparison between numerical and experimental results can be found in Lin and Ebadian [11,12]. Within the investigated parameter ranges, it was estimated that the maximum deviation between the present numerical results and the experimental results is about 5%.

All the numerical computations in this paper were carried out on a Sparc20 Sun Workstation at the Hemispheric Center for Environmental Technology (HCET) at Florida International University. Approximately 350 to 400 iterations were required to obtain converged numerical results.

5. Results and discussion

Most of the data presented in the following sections were obtained under the conditions of $R_c/a = 20$ and $T_w = 10 + T_0$.

5.1. Velocity and temperature fields

The development of the nondimensional axial velocity, U_s, is shown in Fig. 3. On a plane with a small non-

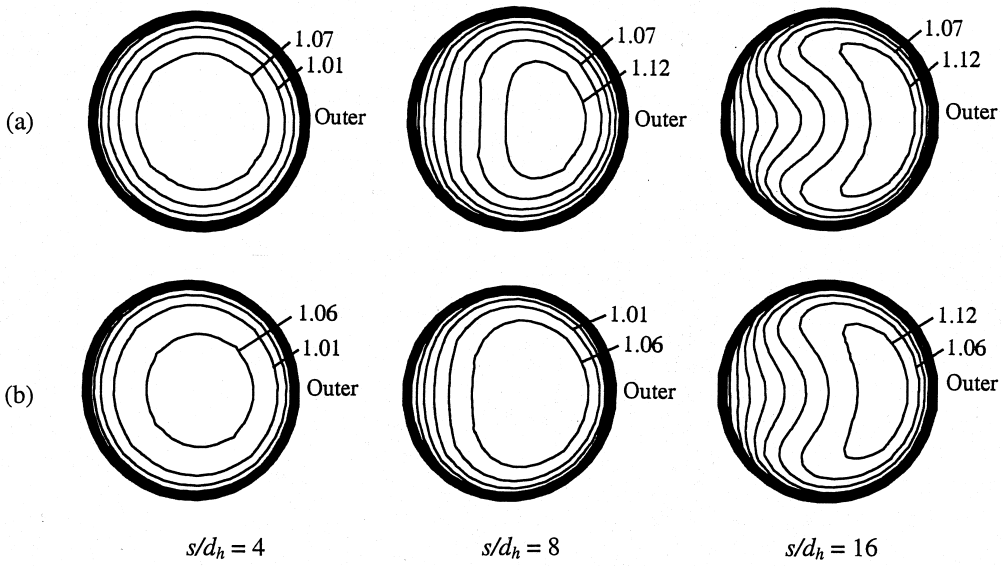

Fig. 3. Development of the axial velocity fields at $Re = 10^4$ and $Pr = 7$: (a) $I = 2\%$; (b) $I = 40\%$.

dimensional axial distance s/d_h, fluid with uniform velocity occupies most of the area of the cross section (the main potential core). As s/d_h increases, the displacement effect of the growing boundary layer accelerates the flow in the main core. The unbalanced centrifugal force of the main flow results in the shift of the point of maximum velocity to the outside of the pipe, forming steeper gradient of U_s near the outer wall. As shown in Fig. 3, the effect of the inlet turbulence level, I, is to reduce the velocity gradient on each cross section. It has been found that the maximum axial velocity on each cross section is barely affected by the increase of the inlet turbulence level.

Figure 4 shows the development of the nondimensional secondary velocity, U_{2nd}. As the effects of inlet turbulence on the secondary flow were found to be very weak within the investigated parameter ranges, typical secondary flow results at only one level of inlet turbulence are presented in Fig. 4. On a plane near the entrance, a weak secondary flow is induced due to the effects of curvature, with one of the vortex cores near the top and the other near the bottom of the cross section. As s/d_h increases, the intensity of the secondary flow increases. It has been found that with the increase of the inlet turbulence level, the two-vortex secondary flow pattern remains unchanged, but the intensity of the secondary flow will reduce slightly. When I is increased from 2 to 40%, the maximum decrease in the secondary velocity is only about 1% on the different cross sections.

Figure 5 demonstrates the development of the nondimensional temperature, Θ. At different axial locations, the temperature field is symmetric to the centerline connecting the outermost and innermost points of the cross section. When s/d_h is small, a fluid of uniform tem-

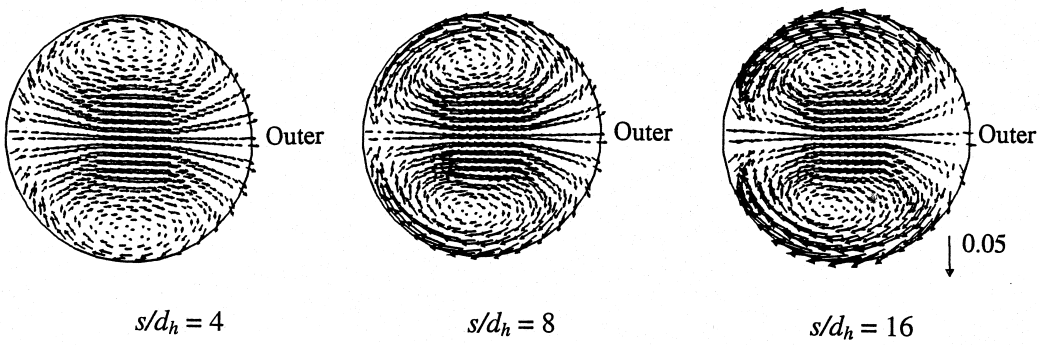

Fig. 4. Development of the secondary velocity fields at $Re = 10^4$, $Pr = 7$ and $I = 40\%$.

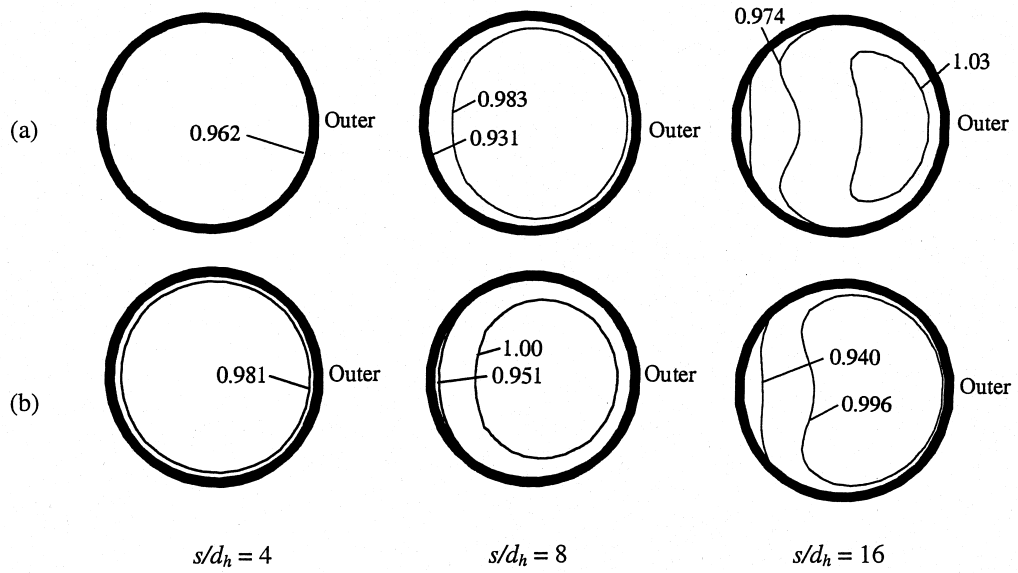

Fig. 5. Development of the temperature fields at $Re = 10^4$ and $Pr = 7$: (a) $I = 2\%$; (b) $I = 40\%$.

perature occupies most of the area of the cross section. As s/d_h increases, the shift of the maximum axial velocity results in a shift of the maximum Θ toward the outside of the pipe, forming steeper Θ gradients near the outer wall. The increase of the inlet turbulence level results in an increase in the developing speed of the thermal boundary layer along the wall of the pipe. With the increase of I, the values of the maximum Θ at different s/d_h change at different levels. When I increases from 2 to 40%, the maximum Θ increases 1.98, 2.91 and 2.78% at $s/d_h = 4$, 8 and 16, respectively.

5.2. Turbulent kinetic energy

The effects of I on the development of the non-dimensional bulk turbulent kinetic energy, k_b, are given in Fig. 6. The bulk turbulent kinetic energy develops rapidly only within a short axial distance from the entrance ($s/d_h < 15$). This rapid developing region is also termed the early developing stage. Usually, the value of k_b increases with the increase of I in the rapid developing region. When $s/d_h > 30$, the bulk turbulent kinetic energy remains a constant value, $k_{b,\infty}$, all the way to the outlet. This phenomenon reveals that the inlet turbulence level has no effect on the bulk turbulent kinetic energy in regions far enough from the entrance of the pipe. The value of $k_{b,\infty}$ depends only on the Reynolds number, Re, and the Prandtl number, Pr. It has been found that the higher the Reynolds number, the lower the value of $k_{b,\infty}$.

Within the rapid developing region, the bulk turbulent kinetic energy, k_b, at different levels of I experiences different behaviors before it reaches the magnitude of $k_{b,\infty}$. Figure 6 indicates that with the increase of s/d_h, k_b at $I = 2\%$ develops from a lower level to a higher level until it approaches the value of $k_{b,\infty}$, while k_b at $I \geqslant 10\%$ falls from a higher level to a lower level until it reaches the value of $k_{b,\infty}$. Interestingly, it is found that at different levels of I, k_b starts from different values at the entrance, however, it reaches the values of $k_{b,\infty}$ at almost the same axial location.

5.3. Friction factor

The development of the circumferential average friction factor, f_m, with axial distance is depicted in Fig. 7. The development of f_m has been found to be oscillatory after a rapid developing region ($s/d_h < 5 \sim 10$), where f_m drops sharply as s/d_h increases due to the rapid development of the flow boundary layer. It has been ascertained that the oscillation of f_m is a consequence of the secondary flow. A similar oscillatory development of the friction factor was also found by Liu [24] in his parabolic numerical study of the laminar developing flow in helical pipes.

In the rapid developing region, except the case of lower values of I and Re (e.g., $I = 2\%$ and $Re = 10^4$), an increase in the level of I results in an increase in the value of f_m at each axial distance. Moreover, with the increase of the level of I, the point of the minimum value of f_m moves downstream.

The effects of I on the oscillation of friction factor, f_m, is found to be weak in this study. As shown in Fig. 7, depending on the value of Re, the effect of I on f_m within the oscillatory stage is different at different axial

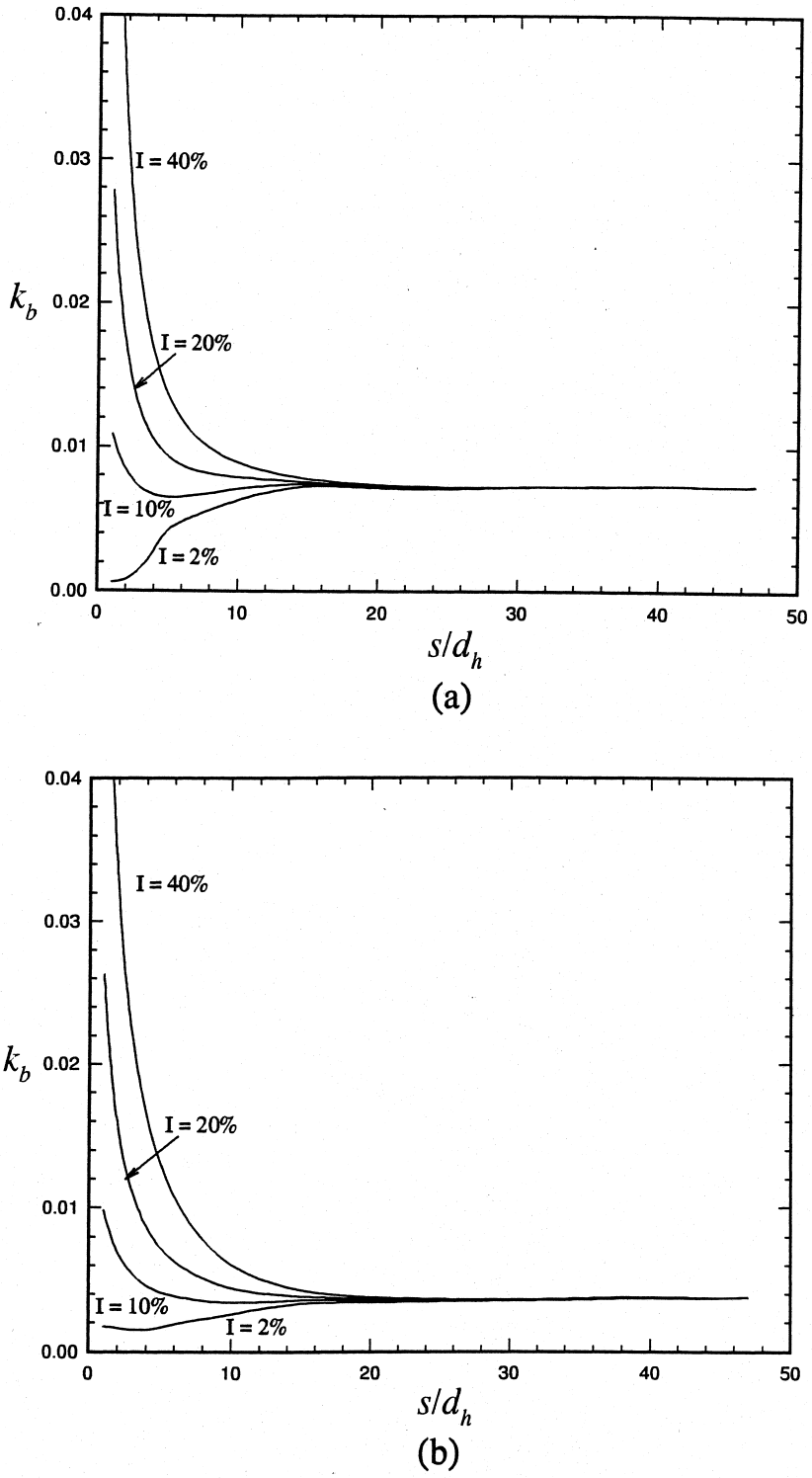

Fig. 6. Effects of inlet turbulence on the development of bulk turbulent kinetic energy at $Pr = 7$: (a) $Re = 10^4$; (b) $Re = 10^5$.

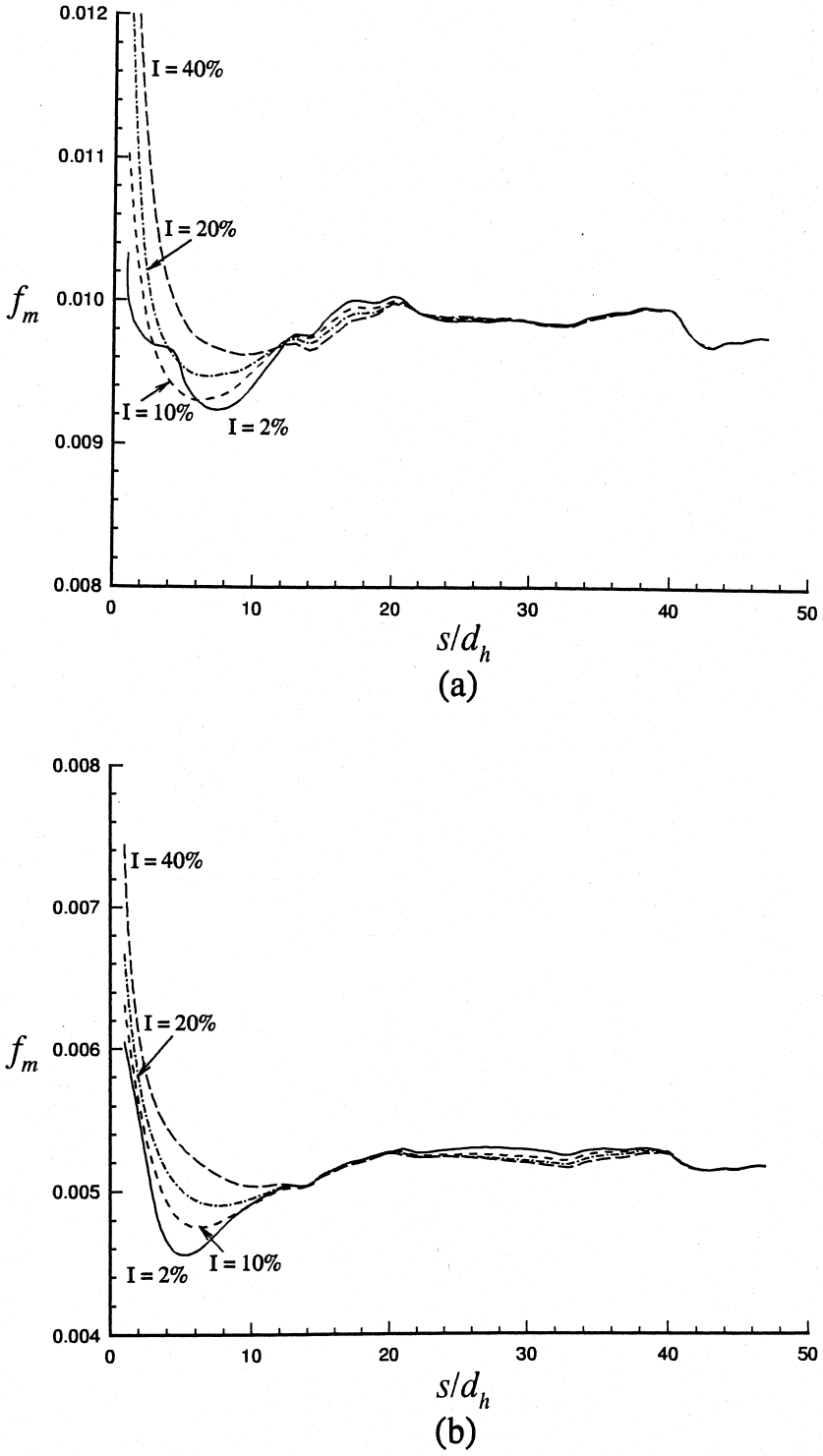

Fig. 7. Effects of inlet turbulence on the development of the average friction factor at $Pr = 7$: (a) $Re = 10^4$; (b) $Re = 10^5$.

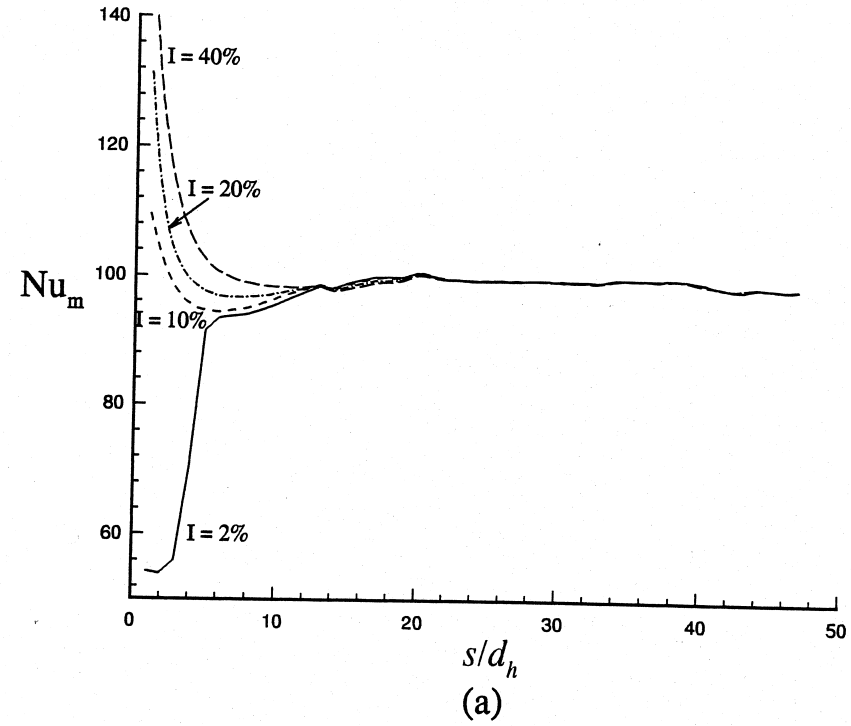

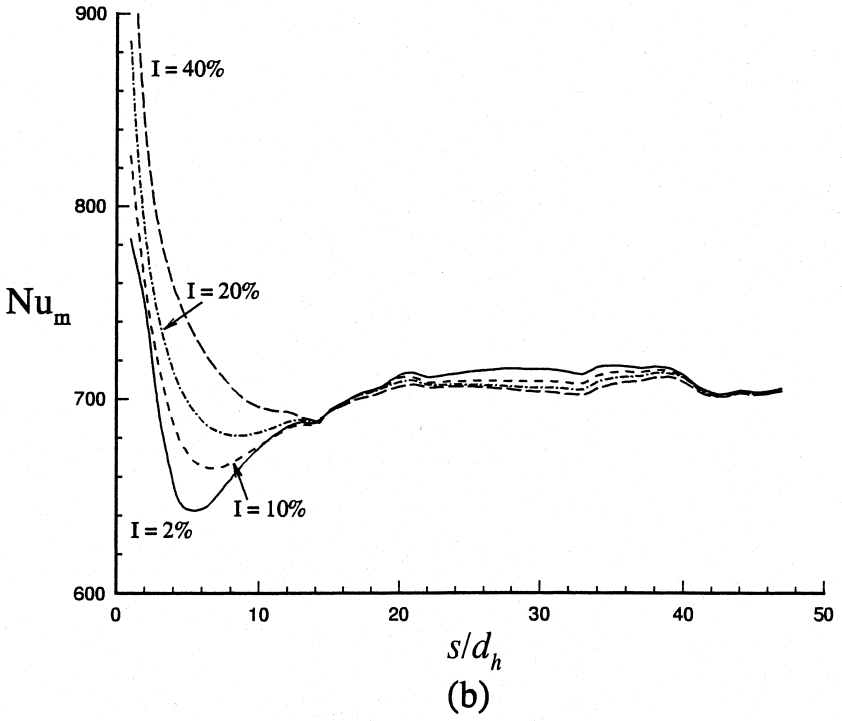

Fig. 8. Effects of inlet turbulence on the development of the average Nusselt number at $Pr = 7$: (a) $Re = 10^4$; (b) $Re = 10^5$.

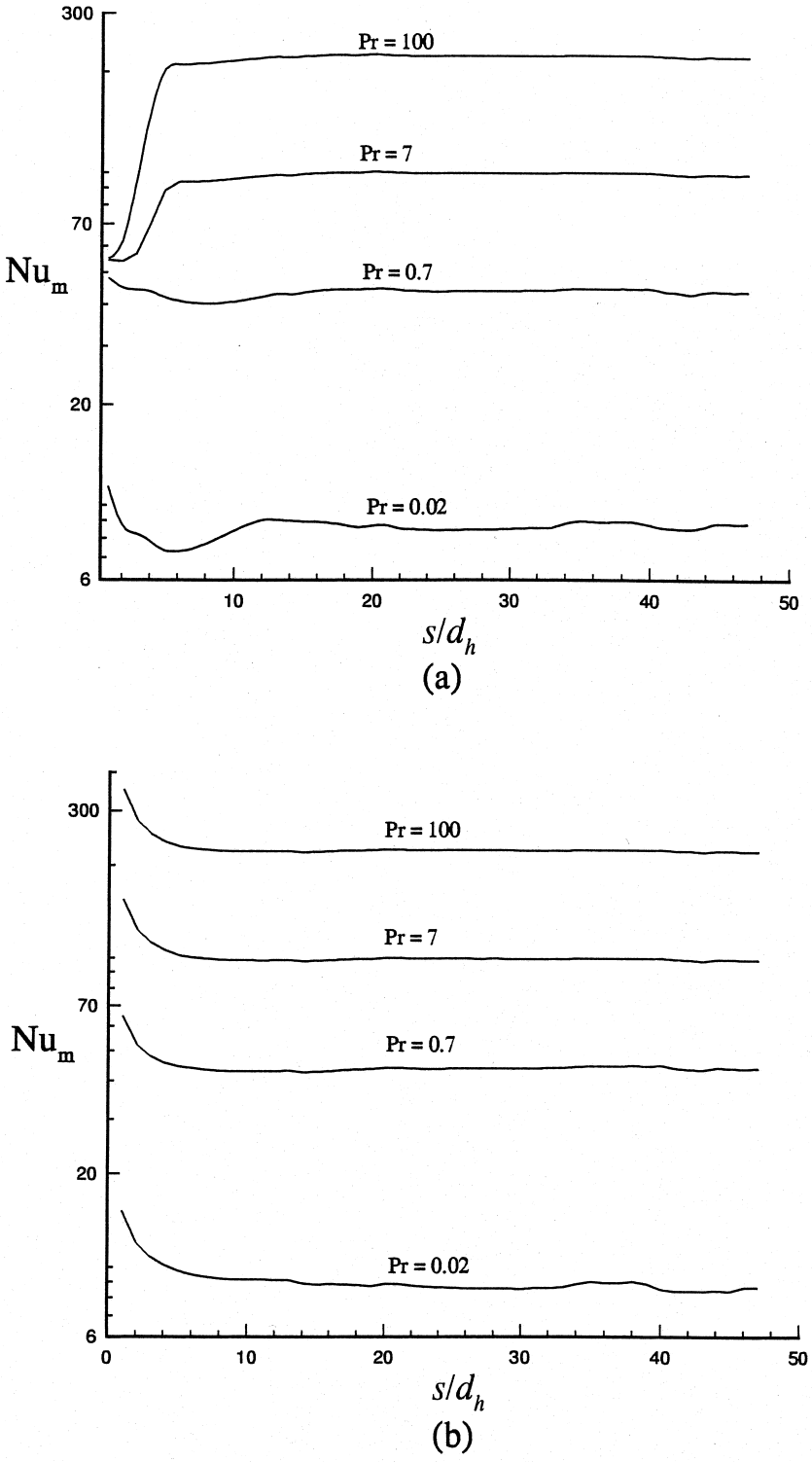

Fig. 9. Development of the average number as a function of *Pr* at $Re = 10^4$: (a) $I = 2\%$; (b) $I = 40\%$.

locations. It is observed from Fig. 7 that before entering the oscillatory stage the friction factors at different inlet turbulence usually tend to merge at a point of $s/d_h \approx 13$–14. After this merging point, the friction factors will diverge with the increase of s/d_h. At another point downstream, the friction factors will merge again. This merging-diverging phenomenon of friction factors at different inlet turbulence level is one of the macro behaviors of the oscillating turbulent flow in the coiled pipe.

5.4. Nusselt number

The development of the circumferential average Nusselt number, Nu_m, with axial location is depicted in Fig. 8. In the rapid developing region ($s/d_h < 5 \sim 10$), except in the case of lower values of I and Re (e.g., $I = 2\%$ and $Re = 10^4$), Nu_m drops sharply as s/d_h increases due to the rapid development of the thermal boundary layer. After the rapid developing region, Nu_m experiences an oscillatory stage, which is similar to that for f_m. It has been ascertained that the oscillation of Nu_m is also a consequence of the secondary flow in helical pipes. Similar oscillatory development of the Nusselt number was found by both Liu [24] and Patankar et al. [25] in their parabolic numerical studies of laminar developing heat transfer in helical pipes.

In the rapid developing region, an increase in the level of I results in an increase in the value of Nu_m at each axial location due to the increased turbulent heat fluxes. Similar to the results of f_m, the point of the minimum value of Nu_m moves downstream with the increase of the inlet turbulence level. The effects of I on the oscillation of Nu_m are also found to be weak, as can be observed in Fig. 8.

The effect of I within the oscillatory stage depends on the value of the Reynolds number. As shown in Fig. 8, within the oscillatory region, the increase of Reynolds number causes the increase in the difference between the Nusselt numbers at different inlet turbulence. It is also found that the higher the Reynolds number, the longer the oscillatory region.

Figure 9 demonstrates the development of Nu_m at different values of the Prandtl number, Pr. With an increase of the Prandtl number, the value of Nu_m at each axial distance increases, and the oscillation of Nu_m is weakened. Two cases of lower I values and higher Pr values ($I = 2\%$, $Pr = 7$ and $I = 2\%$, $Pr = 100$) at $Re = 10^4$ are provided in Fig. 9a to illustrate the distinguishing feature of the development of Nu_m in the rapid developing region found in this study. In these two cases, the development of Nu_m occurs from the lower level to the higher level in the rapid developing region, which is different from the other cases. This unusual development of Nu_m is generated thanks to the extreme low level of inlet turbulence intensity. At this low level of turbulence, the predictions are beyond the capability of the standard k–ε two-equation turbulence model, which is more suitable to high Reynolds number flows with high turbulence level.

6. Conclusions

- The effects of the inlet turbulence level on the development of three-dimensional turbulent flow and heat transfer in helically coiled pipe have been studied by conducting fully elliptic numerical computations with a Control-Volume Finite Element Method.
- The increase of the inlet turbulence level weakens the developing secondary flow velocity and speeds up the development of the thermal boundary layer in the pipe.
- The level of the bulk turbulent kinetic energy is not affected by the inlet turbulence level far enough away from the entrance of the pipe.
- Significant effects of inlet turbulence level on the development of the friction factor and the Nusselt number are limited to the early developing stage of turbulent flow and heat transfer.
- When the inlet turbulence level is very low, abnormal development of Nusselt number may occur in the region near the entrance of the pipe, depending on the Reynolds number and the Prandtl number. This anomalous behavior of Nusselt numbers need to be further investigated.

Acknowledgement

The authors gratefully acknowledge the financial support of the National Science Foundation (NSF) under Grant No. CTS-9017732.

References

[1] C.E. Kalb, J.D. Seader, Entrance region heat transfer in a uniform wall-temperature helical coil with transition from turbulent to laminar flow. Int. J. Heat Mass Transfer 26 (1983) 23–32.
[2] V.A. Mikaila, P.S. Poskas, Local heat transfer in coiled tubes at high heat fluxes (1. Experimental unit, technique and results of preliminary experiments). Heat Transfer—Soviet Research 22 (1990) 713–727.
[3] M.Y.Belenkiy, M.A. Gotovskiy, Y.V. Simonov, B.S. Fokin, Convective heat transfer in steeply bent coils. Heat Transfer—Soviet Research 22 (1990) 595–602.
[4] D.R. Webster, J.A.C. Humphrey, Experimental observation of flow instability in a helical coil. Journal of Fluids Engineering 115 (1993) 436–443.
[5] S.K. Das, Water flow through helical coils in turbulent condition. Canadian Journal of Chemical Engineering 17 (1993) 971–973.
[6] B.K. Rao, Turbulent heat transfer to power-law fluids in

helical passages. Int. J. Heat Fluid Flow 15 (1994) 142–148.
[7] B.K. Rao, Turbulent heat transfer to viscoelastic fluids in helical passages. Exp. Heat Transfer 6 (1993) 189–203.
[8] S.V. Patankar, V.S. Pratap, D.B. Spalding, Prediction of turbulent flow in curved pipes. J. Fluid Mech. 67 (1975) 583–595.
[9] G. Yang and M.A. Ebadian, Turbulent forced convection in a helicoidal pipe with substantial pitch. Int. J. Heat Mass Transfer 39 (1995) 2015–2022.
[10] S.V. Patankar, D.B. Spalding, A calculation procedure for heat, mass and momentum transfer in three-dimensional parabolic flows. Int. J. Heat Mass Transfer 15 (1972) 1787–1806.
[11] C.X. Lin, M.A. Ebadian, Turbulent developing fluid flow in helical pipes. Proceedings of ASME National Heat Transfer Conference, Houston, HTD-Vol. 324, 1996, pp. 65–72.
[12] C.X. Lin and M.A. Ebadian, Developing turbulent convective heat transfer in helical pipes, Proceedings of ASME Winter Ann. Meeting, Atlanta, HTD-Vol. 333, 1996, pp. 77–84.
[13] B.E. Launder, D.B. Spalding, Mathematical Models of Turbulence, Academic Press, London, 1972.
[14] B.E. Launder, D.B. Spalding, The numerical computation of turbulent flows, NTIS N74-12066, Imperial College of Science and Technology, 1973.
[15] P.S. Srinivasan, S. Nandapurkar and F.A. Holland, Friction factors for coils. Tran. Inst. Chem. Eng. 48 (1970) T156–T161.
[16] B.R. Baliga, S.V. Patankar, A control volume finite-element method for two-dimensional fluid flow and heat transfer, Numer. Heat Transfer 6 (1983) 245–261.
[17] Fluent Inc., User's Guide for FLUENT/UNS & RAMPANT, 4th ed., Vols. 1–4, Fluent Inc., Lebanon, NH, 1996.
[18] J. Dormaal, G.D. Raithby, Enhancements of the SIMPLE method for predicting incompressible flow problems. Numer. Heat Transfer 7 (1984) 147–158.
[19] B.R. Hutchinson and G.D. Raithby, A multigrid method based on the additive correction strategy, Numer. Heat Transfer 9 (1986) 511–537.
[20] L.R. Austin, J.D. Seader, Entry region for steady viscous flow in coiled circular pipes, AIChE J. 20 (1974) 820–822.
[21] Y. Mori, W. Nakayama, Study on forced convective heat transfer in curved pipes. Int. J. Heat Mass Transfer 10 (1967) 37–59.
[22] H. Ito, Friction factors for turbulent flow in curved pipes. J. Basic Eng. 82 (1959) 123–132.
[23] G.F.C. Rogers, R.Y. Mayhew, heat transfer and pressure loss in helically coiled tubes with turbulent flow. Int. J. Heat Mass Transfer 7 (1964) 1207–1216.
[24] S. Liu, Laminar flow and heat transfer in helical pipes with finite pitch, Ph.D. thesis, University of Alberta, Canada, 1992.
[25] S.V. Patankar, V.S. Pratap, D.B. Spalding, Prediction of laminar flow and heat transfer in helically coiled pipes. J. Fluid Mech. 62 (1974) 539–551.